5-2018

pH Sensitivity of Connexin 50 Hemichannels: H95 and Beyond

Leah Volk
volklm01@mail.buffalostate.edu

Advisor
Derek Beahm, Ph.D
First Reader
Derek Beahm, Ph.D.
Second Reader
I. Martha Skerrett, Ph.D.
Third Reader
Gregory Wadsworth, Ph.D.
Department Chair
I. Martha Skerrett, Ph.D.

pH Sensitivity of Connexin 50 Hemichannels: H95 and Beyond

by

Leah Volk

An Abstract of a Thesis in Biology

Submitted in Partial Fulfillment
of the Requirements
for the Degree of

Master of Arts

May 2018

Buffalo State College
State University of New York
Department of Biology

ABSTRACT OF THESIS

Gap junction channels formed by connexin proteins are critical for the health and function of the vertebrate lens. It is important to understand how these channels are affected by pH because a pH gradient exists in lens tissue. Intracellular pH (pH_i) is a regulator of gap junction coupling, and different connexins show different sensitivities to pH_i. A "Particle-Receptor" model for pH-dependent channel closure involves the intramolecular interaction between the cytoplasmic tail of the connexin and a region near the mouth of the channel dependent on a highly conserved histidine residue at position 95. While this model explains the pH sensitivity of some connexins, removal of H95 or truncation of the C-tail does not affect the lens connexin, Cx46. The goal of this thesis was to explore the roles of histidines residues located at and near position 95 for the other lens connexin, Cx50. Site-directed mutagenesis was used to replace single or combinations of histidine residues. Functional assays of Cx50 wildtype and mutant hemichannels were examined by electrophysiological techniques in the *Xenopus laevis* heterologous expression system. Preliminary findings suggest that H95 may not be necessary for pH-dependent channel closure. Attempts to determine if nearby histidine residues could act as redundant sensors were inconclusive due to poor expression levels. I show that removing all three histidine residues resulted in little to no channel activity despite the protein being trafficked to the plasma membrane. Ongoing experiments on these mutants will help identify the structural determinants of pH sensitivity in Cx50 channels.

pH Sensitivity of Connexin 50 Hemichannels: H95 and Beyond

by

Leah Volk

A thesis submitted in Partial
Fulfillment of the Master of Arts degree
in Biology at Buffalo State College

May 2018

Approved by:

Derek Beahm, Ph.D.
Assistant Professor
Chairperson of the Committee
Thesis Adviser

I. Martha Skerrett, Ph.D.
Associate Professor and Chair
Department of Biology

Kevin J. Miller, Ed.D.
Dean
The Graduate School

THESIS COMMITTEE

Derek Beahm, Ph.D.
Assistant Professor of Biology

I. Martha Skerrett, Ph.D.
Associate Professor and Chair

Gregory Wadsworth, Ph.D.
Associate Professor

LIST OF TABLES

LIST OF FIGURES

TABLE OF CONTENTS

Introduction and Background

Physiological Role of Connexins in the Vertebrate Lens

Gap junctions are instrumental in maintaining the clarity and health of the vertebrate lens. Mutations in the connexin genes that encode the lens fiber cell gap junction proteins Cx50 or Cx46 have been shown to cause cataracts, and neither of the connexins can separately sustain a normal lens, as evidenced by knockout studies (Gong et al., 1997; White et al., 1998). Lens gap junction channels are thought to play a role in maintaining and directing a pattern of ion flow to establish an internal circulation system in the lens (Mathias et al, 2007). In this model, a sodium current enters lens fiber cells from the extracellular spaces and is redirected out to the equator of the lens through gap junction channels that connect the fiber cells. Driven by osmotic forces, a large volume of water, facilitated by aquaporin water channels, accompanies the current flow and contributes to generating a hydrostatic pressure within the lens. A measurement of hydrostatic pressures within wild-type mouse lenses showed that pressure dropped by approximately 1 mmHg across each layer of gap junctions, with a maximum pressure of 328 mmHg at the center of the lens. In this study, mice with reduced numbers of gap junctions in the fiber cells showed a marked and linear decrease in the hydrostatic pressure gradient within the tissue (Gao et al, 2011). This can be taken as evidence that gap junctions are an essential part of the hydrostatic fluid flow within the lens which acts as a replacement for the circulatory system found in other tissues for nutrient delivery and waste removal.

The role of connexins in the lens may be more complicated because some connexins are known to function as hemichannels in nonjunctional plasma membrane. Cx50 is found predominantly in the fiber cells of the lens of the eye, and has been shown to form functional hemichannels when expressed in single oocytes (Ebihara and Steiner, 1993; Zampighi et al.,

1999; Beahm and Hall, 2002). While there is no direct evidence, this means that hemichannels in the lens could potentially contribute to the transmembrane sodium current that is an integral part of the above model. There is in-vivo evidence of roles for hemichannels in other tissues of the eye. Shahidullah and Delamere (2014) provided evidence for this by injecting the aqueous humor compartment of porcine eyes with propidium iodide (PI). The dye was shown to flow into the nonpigmented ciliary epithelium in a process that could be blocked by both calcium and a connexin antagonist, strongly suggesting hemichannels as the primary transporter between the aqueous humor and the ciliary epithelium.

Factors that affect the ability of gap junction channels, and possibly their component hemichannels, to open and close will influence their role in normal physiology. The gap junctions expressed in the fiber cells of the lens tissue exhibit pH-dependent gating, which may be physiologically relevant due to the pH gradient existing in this tissue, in which the core of the lens is more acidic than the periphery. The purpose of this thesis was to explore the possible mechanism by which pH closes Cx50 channels.

Overview of Gap Junction Structure and Function

Gap junctions are important in all multicellular animals, serving a variety of functions in different tissues of the organism by virtue of allowing cells to directly communicate with each other. The basic structure of gap junction channels, from protein to hemichannel to complete gap junction channel, is shown in Figure 1. Gap junctions are comprised of a few to thousands of individual channels that form across two cell membranes, linking the cytosolic compartments of neighboring cells to facilitate the exchange of ions, metabolites, and other small molecules (Goldberg et al, 2004). Each half of the junction is known as a hemichannel, which is in turn made up of six connexin subunits (Harris and Locke, 2009). These connexin subunits can be

identical, resulting in a homomeric hemichannel, or varied, resulting in a heteromeric hemichannel. The six subunits assemble to form the central conducting pore through which ions and small molecules may pass. Hemichannels from cells in contact will dock end-to-end to form the gap junction channel which connects the cytosolic compartments of the cells through a continuous central pore.

There are 21 connexin genes in the human genome, and 20 in the mouse (Pfam accession number PF00029. http://pfam.sanger.ac.uk/family?acc=PF00029). They code for a family of membrane proteins that have four transmembrane (TM) domains, with the amino and carboxyl terminus both in the cytosol. Connexins share sequence homology in several key areas, with most of the variation occurring in the cytoplasmic loop and C-terminal tail. The C-terminal domain of connexins has been shown to affect the pH and calcium dependent gating of these channels, notably in heart tissue and the lens of the eye (Xu et al, 2002, Sahu and Bera, 2013). The N-terminal domain also influences several important physiological properties of gap junctions, including oligomerization and voltage gating (Gemel et al, 2006).

Gap junctions play a critical role in the normal function of a tissue. The large aqueous pore characteristic of a gap junction channel allows for the exchange of different types of small ions and molecules which in turn serves different functions. In general, gap junctions are associated with the synchronization of electrical and metabolic activity of cells within a tissue, and can also allow for the propagation of second messenger signals. Mutations in connexins have been linked to several inherited disorders in humans, including hearing loss, heart defects, skin diseases, and cataracts (Kelly et al, 2015).

Gating of Gap Junctions and Hemichannels

Gap junction channels open and close ("gate") depending on a variety of factors, including voltage, intracellular calcium and pH, post-translational modifications, and binding of ligands. All gap junction channels, regardless of the connexin subunits, display voltage-dependent gating (Goldberg et al, 2004). This type of gating is dependent on V_j, the transjuctional voltage, and involves both a fast gate and a slow gate. A difference between the membrane potentials of two cells creates a transjunctional voltage which can close the gap junction channel. Most gap junction channels do not close completely in response to voltage, but instead reside in a lower conductance state, or G_{min} (Harris and Locke, 2009). A variety of mutations have been shown to attenuate the charge selectivity, voltage gating, and the overall function of the Cx50 gap junction channel. These include D47H and L7Q (Liska et al, 2008; Li et al, 2013), which both resulted in cataract, several mutations of G46 (Tong et al, 2014), which was shown to be important in unitary conductance and transjunctional voltage-dependent gating, and S276F (Liu et al, 2015), which resulted in a non-functional channel.

In addition to voltage gating, gap junction channels have varying sensitivities to changes in intracellular $[Ca^{2+}]$ or $[H^{+}]$, where channel closure occurs with increased calcium or decreased pH. This is referred to as 'chemical gating'. The current mechanism for calcium sensitivity involves calmodulin (CaM) as an intermediate between the calcium and the connexins themselves (Peracchia, 2004). The current mechanism for pH sensitivity appears to vary with connexin type and will be discussed shortly as the main subject of this thesis.

At this point, it is important to understand that some types of hemichannels can gate independently into the extracellular space, and have been implicated in several physiological processes, including in the ciliary epithelium of the eye and astrocytes of the brain (Shahidullah

and Delamere, 2014; Ye et al, 2003). The gating and permeability properties of hemichannels have been shown to reflect those of gap junctions, including pH and calcium sensitive gating (Saez et al, 2005; Srinivas et al, 2005). Open probability of hemichannels is increased by depolarized membrane potentials and low extracellular calcium, as well as several types of chemical modifications (Sáez et al, 2005). Bao et al (2004) found that phosphorylation of Cx46 affects open probability in a predictable fashion, in that an upregulation of PKC is followed by a decrease in permeability. When the sites of phosphorylation in Cx46 were mutated to alanine, the channels remained open and cell swelling was observed.

Given that hemichannel properties often reflect those of their complete gap junction channels, they are sometimes used as a more accessible tool for studying gap junctions because it is easier to conduct electrophysiological experiments on single cells compared to pairs of cells.

pH-dependent Gating of Gap Junction Channels and Hemichannels

Gap junction channels show sensitivity to intracellular pH, closing in a more acidic environment which presumably could help uncouple a healthy cell from an unhealthy one. In Cx43, the pH dependent gating process of gap junctions has been shown to involve interactions between two different regions of the connexin protein. Specifically, upon intracellular acidification, the cytoplasmic tail is thought to interact with a protonated histidine residue at position 95 (H95) that resides near the channel mouth. This mechanism is described using a "particle-receptor" or "ball-and-chain" model whereby the C-tail of Cx43 serves as the particle or ball and the H95 region serves as the receptor.

The ball and chain model for pH dependent closure of Cx43 gap junction channels was supported by a series of publications. The first experiments expressed Cx43 and Cx32 in oocytes, which were paired and then voltage clamped (Liu et al, 1993). Cx43, with a protein pK_a of 6.6

(calculated from the Hill coefficient), exhibited an increase in conductance in a narrow range of pH, whereas Cx32 and Cx43 M237 (a truncation mutant of Cx43) had more acidic pK_a and steeper Hill coefficients. These data indicated that the sensitivity of these connexins to acidification could have a structural basis. To further understand the molecular basis of the pH sensitivity of this channel, the H95 of Cx43 was mutated to a series of different residues, which either attenuated or ablated pH sensitivity of the channel (Ek et al, 1994). Targeted deletions were then performed on the carboxyl tail to elucidate the regions which interact with H95 (Ek-Vitorín et al, 1996). Finally, the tail was expressed independently along with other connexin channels and was shown to confer pH dependence (Morley et al, 1996). This series of papers outlines the mechanism by which Cx43 gates in response to pH. Later experiments showed that histidine residues in the cytoplasmic loop can alter the structure of the loop in a pH-dependent manner, and that this region serves as the receptor region for the tail (Duffy et al, 2002). Protonation of H95 is considered important in that it contributes to the conformational changes in the C-loop needed to interact with the tail. It is unclear as to what extent this model applies to the pH dependent closure of gap junction channels composed of other hemichannels.

Previous work on the pH-sensitive Connexin 43 gap junction channels has shown that the mutation of H95 to lysine (K) increased pH sensitivity, causing the channel to close at a higher pH than the wildtype Cx43 (Ek et al, 1994). In contrast, the mutation to tyrosine (Y) and aspartic acid (D) reduced the channel's pH sensitivity, such that a lower pH was necessary to induce closure. This suggests that positive charges are associated with closing of gap junctions, which may be acting at the level of hemichannels. These substitutions have an attenuating effect rather than causing complete loss of pH sensitivity. The mutation of H95 to glutamine (Q) formed non-functional channels that were rescuable by the introduction of nearby histidines (Ek et al, 1994).

This H95 has been shown to be the site of interaction with the C-terminal tail in Cx43 and is the receptor in the "ball-and-chain model" discussed earlier. The H95 residue sits at the interface between the second transmembrane domain and the first intracellular loop, which is associated with the central pore (Ek et al, 1994). It is possible that this region acts as a pH sensor in Cx50 as well.

The lens connexins and pH dependence

Like most connexins, the lens fiber cell connexins (Cx46 and Cx50) form gap junction channels that also close upon cytoplasmic acidification. A comparison of gap junction channels based on pKa (the pH at which the normalized conductance (or G_j) is at 50% of maximum) reveals that among the connexins, Cx50 is the most sensitive to acidification, with a pKa of 7.2 (Stergiopoulos et al, 1999). Trexler et al (1999) studied the pH sensitivity of Cx46 hemichannels, using both whole cell and single channel techniques. They mutated H95 to aspartic acid as well as cysteine and did not see a reduction in pH sensitivity as was seen in Ek et al. Additionally, they removed the cytoplasmic tail and continued to observe closure of the channel in response to acidification. This suggests that the lens connexins may have a different pH gating mechanism than Cx43 and Cx40, which were the basis of Delmar's 'particle and receptor' model. The sequence of Cx46 does reveal an H98, which is also present in Cx50. This residue could also play a role in Cx46's pH sensitivity, given its proximity to H95, but was not altered to test this hypothesis.

Native Cx50 is cleaved at the cytoplasmic tail when expressed in the human lens, possibly to allow the gap junction to remain open in the acidic core of the tissue. Different studies have produced varying results in regard to the pH sensitivity of truncated Cx50. Some have shown loss of pH sensitivity (DeRosa et al, 2006; Xu et al, 2002), while others have shown

little to no loss (Stergiopoulos et al, 1999). This discrepancy may be due in part to the fact that different isoforms of the protein from different species have different calpain cleavage sites, thus leading to conflicting data (Wang and Schey, 2009). Our recent experiments in Xenopus oocytes with truncated Cx50 suggest that pH dependent gating of the hemichannels may not require the full tail (unpublished data).

Cx50 hemichannels were shown to be sensitive to extracellular pH, closing completely at external pH 6.0 (Beahm and Hall, 2002). These hemichannels are also sensitive to intracellular pH (Zampighi, 1999: Sáez et al, 2005). The mechanism of hemichannel pH gating in response to extracellular pH remains unexplored, but could reflect the gap junction pH gating mechanism triggered by proton entry through open hemichannels. In any case, the pH sensor for channels formed by the lens connexins remains a mystery.

pH Gating of Other Channels

Histidines act as a pH sensor in other channels, likely due to their ability to change protonation state within a physiological pH range. Triads or even larger groups of histidines have been shown to participate in the pH-sensitive opening and closing of channels by the protonation and distribution of charges throughout the imidazole rings (Hu et al, 2006). When exposed to low pH, these histidines would become positively charged, generating a positive 'sticky patch' on the inside of the channel. In the influenza A virus, the protonation of the M2 proton channel is associated with its opening whereby a ring of histidines within the channel change conformation upon protonation and allow H^+ ions to flow through the pore (Hu et al, 2006). The water channel Aquaporin 0 has been shown to be sensitive to external pH whereupon acidification increases the channel's water permeability (Németh-Cahalan, 2004). The molecular basis for this property has been shown to rely on histidines in the A and C loops of the channel,

and replacing or shifting these residues can attenuate the pH sensitivity of this channel from acidic to alkaline. Aquaporin 4 also contains a histidine at position 95 which acts as a pH sensor (Kaptan et al, 2015). Interestingly, H95 appears to be conserved among the aquaporin family in a manner similar to the connexin family. Upon protonation of the histidine residue, which exists at the narrowest region of the channel, structural changes occur which open the channel and this effect is eliminated upon mutation of the histidine to the non-pH sensitive alanine (Kaptan et al, 2015).

In other channels, pH sensitivity can be a consequence of mechanisms unrelated to histidine residues. A recent study of the Kir1.1 channel proposed that the pH sensor is not a set of particular residues unique to pH-sensitive Kir channel, but instead integrated within the common gating mechanism of all Kir channels (Paynter et al, 2010). This model proposes that all Kir channels contain the residues necessary for pH sensitivity, and that the subclass of channels which exhibit this gating have subtle structural changes which bring this sensitivity into the physiological range. Also, while not involving a histidine, Cx26 employs a similar method of protonation of a residue with resultant structural changes in response to pH. Specifically, in neutral conditions, the Asp2 and Met1 of neighboring connexins associate and block the pore, but upon acidification, Asp2 is protonated and disassociates from Met 1, rearranging the N-terminal helices to open pore (Wang et al, 2011).

Thesis Goal

The sequence of mouse Cx50 reveals a unique pattern of three histidine residues at positions 95, 98 and 99 which are not found in other members of the connexin protein family, as shown in Table 1. This unique pattern is conserved in the majority of Cx50 orthologs found in other species, as shown in Table 2. Cx50 primary sequence is shown with membrane topology

in Figure 2, where the histidine residues of interest are highlighted to occur at the cytoplasm-membrane interface of the second transmembrane domain. Figure 3 shows a helical wheel model of the second transmembrane domain of several connexins, including Cx50, to demonstrate that the positioning of the 3 histidine residues in Cx50 align to one side of an alpha helix to create what I call a triad. Given that histidines are sensitive to pH-induced changes in the biological pH range, I hypothesize that these may be responsible for the increased pH sensitivity of Cx50.

If the two additional histidines in Cx50 can act similarly to H95 in Delmar's "particle and receptor" model, I expect that the mutation of one, or possibly two, of these histidines will not destroy the pH sensitivity of the channel. Trexler et al's results in Cx46 suggest that lens connexins may be able to use an alternative mechanism involving either H98 (in Cx46) or H98 and/or H99 (in Cx50) or some other, unknown mechanism. In this thesis, I systematically generated mutants of these three histidines, either individually or in combination, to test a hypothesis that these residues may be responsible for the pH-sensitive gating mechanisms of Cx50 channels. These multiple histidines may act in a redundant manner to ensure this connexin remains pH sensitive in the event of a single histidine mutation.

Research Design/Methods

Objective: To examine the functional significance of histidine residues at positions H95, H98, and H99 on the pH dependence of mouse Cx50 hemichannels. Site-directed mutagenesis was used to generate a series of mutations in mouse Cx50 cDNA, followed by in-vitro synthesis of cRNA and protein expression in the Xenopus *laevis* oocyte heterologous expression system. Hemichannel currents were collected using a Two-Electrode Voltage Clamp (TEVC) technique

on oocytes perfused with media containing high concentrations of divalent cations for closed channels, zero-added divalent cations at pH 7.6 for open channels, and zero-added divalent cations at pH 6.0 to assess pH effect on open channels. A Western blot protocol was developed to determine if nonfunctional mutant hemichannel protein reached the plasma membrane.

Isolation of Plasmid DNA

A glycerol stock of E. Coli containing mouse Cx50 wildtype cDNA cloned into a pSP64 plasmid vector was used as the starting material for experiments, and ampicillin was used as a selection marker for bacteria containing the vector. Agar plates made of LB broth supplemented with 100 µg/mL ampicillin were streaked with the glycerol stock and maintained in a 37^{o}C incubator overnight. Individual colonies were used to inoculate liquid LB-Amp broth and cultured overnight in a shaking incubator at 37^{o}C. Plasmid DNA was isolated using the QIAGEN (Hilden, Germany) QIAprep Spin miniprep kit as per manufacturer's instructions and DNA was eluted in 50 µl nuclease-free water. The presence and concentration of plasmid DNA was verified on 1% agarose gels ran at 100V for 25 minutes.

Custom Primer Generation

Primers for mutagenesis contained altered nucleotides flanked by wild-type sequences. The primers bind to wild-type cDNA and the mutation is incorporated into subsequent copies of the DNA by the process of PCR. Primers for mutagenesis and sequencing were designed via the Agilent (Santa Clara, CA) QuikChange Primer Design webpage (link: https://www.genomics.agilent.com/primerDesignProgram.jsp) using sequence information from the NCBI (Gja8 gap junction protein, alpha 8 [Mus musculus (house mouse)], Gene ID: 14616. Link: https://www.ncbi.nlm.nih.gov/gene/14616). The oligonucleotide primers were synthesized, desalted, and provided as a lyophilized stock by Integrated DNA Technologies (Coralville, IA).

The primers were resuspended to a stock concentration of 2.5 µg/µl in nuclease-free water, and then at 25 ng/µl as a working stock. Custom primers for all mutations are described in Table 3.

Site Specific Mutagenesis and Verification

Mutations were produced using the QuikChange Lightning Site Directed Mutagenesis kit from Agilent (Santa Clara, CA), which uses the custom primers described above and PCR to introduce nucleotide changes into the gene of interest. The protocol was followed as per manufacturer's instructions, with the substitution of SOC broth for NZY+ media in the culture of the XL10-Gold ultracompetent cells. The cycling conditions for PCR were: 95°C/ 2 mins initial denaturation, then the following for 20 cycles: 95°C/10s, 60°C/10s, 68°C/2m30s. The final extension was at 68°C for 5 minutes. 2 µl of Dpn (supplied with the site-directed mutagenesis kit) was added to each 50 µl reaction to digest parental DNA. This mutant cDNA was then used to transform competent bacteria to generate clones for stable supply of abundant DNA. 45µl of XL10-Gold Ultracompetent cells were mixed with 2 µl beta mercaptoethanol and incubated on ice for 2 minutes. 2 µl of DNA was then mixed with the cells per reaction and these were incubated on ice for 30 minutes. The cells were then heat-shocked at 42°C for 30s and recovered at 37°C for 1 hr at 225 rpm. Post-transformation, 250 µl cells were streaked on LB-Ampicillin plates and incubated for 17-24 hours at 37°C. Two individual colonies were picked from each plate and inoculated into liquid LB+Amp, and incubated overnight at 37°C. Plasmid DNA purified from these clones was sent to GenScript (Piscataway Township, NJ) for sequencing using both an SP6 promoter region primer and an internal sequencing primer halfway through Cx50 sequence to ensure sequencing the complete reading frame. Sequences were verified via NCBI's ORF Finder tool (Open Reading Frame Finder Tool, National Center for Biotechnology Information, link: https://www.ncbi.nlm.nih.gov/orffinder/) and comparison to the WT sequence.

cRNA Synthesis

Isolated plasmid DNA was linearized with EcoR1 (New England Biolabs, Ipswich, MA) at 37°C for 1 hour using 10 units of EcoR1 per 1 µg of DNA in a 20 µl reaction. Reactions were terminated by heat inactivation at 65°C for twenty minutes. Following verification of the digest on a 1% agarose gel, the linearized DNA was ethanol precipitated and resuspended in 5 µl of nuclease-free water. This DNA was then used for the generation of mutant cRNA via the Ambion mMessage mMachine Sp6 Kit (Fisher Scientific (part of Thermo-Fisher Scientific), Ambion, Inc. brand, Waltham, MA). DNA concentrations were approximated by comparing ethidium bromide staining intensity on a gel to that of a known DNA ladder. About 0.5 – 1 µg of DNA was used per cRNA reaction, along with recommended amounts of other reaction agents as outlined in the manufacturer's protocol. The reaction was allowed to proceed for 5 hours at 37°C due to the relatively slow speed of the Sp6 RNA polymerase resulting in lower yields when shorter reaction times are used. LiCl precipitation of the cRNA as per manufacturer's instructions in the mMessage Machine Kit proceeded for 24 hours at -20°C for maximum yield. Following centrifugation, the cRNA pellet was resuspended in 10 µl nuclease-free water and stored at -20°C for short term or -80°C for long term storage. RNA was verified using 1% agarose gel electrophoresis. An RNA ladder (ssRNA ladder, New England Biolabs, Ipswich, MA) was included on some of the 1% agarose gels to ensure correct size and adequate concentration of RNA.

cRNA Injection into Xenopus laevis Oocytes

Xenopus *laevis* oocytes were stored at 18°C in ND96 medium with supplements (96 mM NaCl, 2 mM KCl, 1 mM $MgCl_2$, 1.8 mM $CaCl_2$, 5mM HEPES pH 7.4, plus 500 mg/L Gentamicin, 100 U/L Penicillin, 100 µg/L Streptomycin, and 2.5 mM sodium pyruvate) which

was changed every 24 hours. PIPES was used instead of HEPES when preparing ND96 solutions at pH values less than 6.5. Oocytes were chemically defolliculated by incubation for 30-45 minutes in a collagenase solution containing a trypsin inhibitor at 2 mg/mL prepared in divalent cation-free ND96.

Oocytes were washed several times in ND96 before selecting Stages V and VI oocytes for injection. Injection needles were pulled from Drummond 7" #3-000-203-G/XL capillary tubes on a Narishige Model PC-10 vertical puller using the 1-step pull setting. Needle tips were then manually broken to a width of 20-30 µm under a dissection microscope. These needles were backfilled with mineral oil and mounted on a Drummond Nanoject 2 injector. The needle tips were filled with 1.5-2 ul of water containing a mix of cRNA (concentrations varied between 50-550 ng/µl) and an antisense oligonucleotide against endogenous Cx38. The mix was prepared so that a 46 nl injection delivered about 5 ng of antisense oligo and 10 ng of cRNA. Approximately 30-40 oocytes were injected with 46 nl of each cRNA/antisense mix, along with the same number of control oocytes receiving only the anti-Cx38 antisense. The injections took place in calcium, magnesium, and antibiotic free ND96, after which the injected oocytes were stored in ND96 with supplements. On some occasions, the media was also supplemented with 1 mM $CoCl_2$ to ensure that hemichannels, if expressed, remain closed.

Voltage Clamping of Injected Oocytes

TEVC (Two Electrode Voltage Clamp) was used to determine if functional hemichannels existed in the plasma membrane and how hemichannels responded to external pH changes. Occytes were voltage clamped using an Axoclamp 2A voltage clamp amplifier, a Digidata 1322 D-A/A-D converter, and PClamp software.

TEVC uses two glass electrodes which are inserted into the oocyte. One electrode monitors the V_m of the oocyte, while the other passes current into the oocyte. With the membrane of the oocyte acting as a resistor, the V_m is measured and current is injected to maintain command voltage. If the channels are open, a large current is required to maintain a selected command voltage, whereas if the channels are closed, little current is needed. Whole cell conductance was determined by measuring the change in current generated by a 10 mV depolarizing voltage step, using the equation $G = \frac{\Delta I}{\Delta V}$.

Voltage recording and current passing electrodes were pulled from borosilicate glass capillary tubes on a vertical needle puller. The needle filling solution was composed of 150 mM KCl, 10 mM EGTA, and 10 mM HEPES, pH 7.4. Needles that had smaller tips and resistances between 1 and 3 MΩ for were used for voltage recording electrodes, while the current passing electrodes had slightly larger tips with resistances of 0.1 to 0.3 MΩ.

Oocytes were held at a holding potential -20 mV, and subjected to a series of 5 sec voltage steps from -110 mV to +50 mV in 20 mV increments. The family of current traces elicited by these voltage steps was stored on the computer for later analysis. Current traces were collected for each oocyte after perfusion with different solutions, including ND96, and divalent cation-free ND96 at pH 7.5 or 6.0.

Western Blot of Membrane Surface Proteins

A Western Blot of surface labelled proteins was used to detect expression and plasma membrane residency of wild-type and mutant Cx50. Six oocytes per injected RNA were incubated in 10mM EZ-Link™ HPDP-Biotin (Thermo-Fisher, Waltham, MA) in DPBS (Dulbecco's Phosphate Buffered Saline, Thermo Fisher Scientific, Waltham, MA) for 30 mins at room temperature with rocking, to label surface protein cysteine residues with biotin. Oocytes

were then washed 3 times in DPBS, and then frozen overnight in 0.5 mL ultrapure dH_2O with 1x Halt Protease Inhibitor (Thermo Fisher, Waltham, MA) at -80°C. Oocytes were thawed on ice, supplemented with 100 ul TE, and homogenized by drawing through a 22-guage needle 10x. The homogenate was spun at 1000xg at 4°C for 10 mins to remove large debris. The top 500 µl of supernatant was added to 500 µl of 2x solubilization buffer (DPBS+0.2% SDS, 2% NP40, 2x Halt Protease Inhibitor (Thermo Fisher, Waltham, MA) in new tubes. Samples were then incubated at 4°C for 2 hours, then spun at 18,000xg at 4°C for 15 mins. Supernatant was transferred to a new tube and biotin labelled plasma membrane proteins were collected by incubation with 50 µl avadin beads (Immobilized NeutrAvidin Gel, Thermo Fisher Scientific, Waltham, MA) overnight at 4°C, after which the beads were pelleted with a 1 min spin at 9000x g. Proteins were removed from the beads by incubating at 95°C for 5 min in a reducing SDS-PAGE loading buffer. Proteins were stored at -20°C prior to running on reducing SDS-PAGE gels.

Protein samples (20 ul/lane) and a protein ladder (3 ul/lane, BIORAD Precision Plus Protein All-Blue Standards) were loaded onto a 10% SDS-PAGE gel and ran at 30V for 5 mins, then 100V for 1.5 hrs. The gel was equilibrated in transfer buffer (25 mM Tris, 192 mM Glycine) for 15 mins and proteins were transferred to a PVDF membrane using a Biorad Mini Trans-Blot Electrophoretic Transfer Cell. Transfer proceeded for 70 min at 300 mA. The membrane was washed in DPBS, and stored overnight at 4°C in blocking solution consisting of DPBS supplemented with 0.05% Tween 20 (DPBS-T) and 5% BSA.

The membrane was warmed to 25°C in blocking solution for 15 mins and then rinsed 3x for 20 mins each in DPBS-T. The membrane was incubated in a 1/100 dilution of Cx50 primary antibody (Cx50, B-11, sc373801, mouse monoclonal IgG_1, 200µg/mL, Santa Cruz

Biotechnology, Dallas, TX) in 10 mL of DPBS-T/2.5% BSA at room temperature with gentle shaking for 1 hr. After rinsing 3x, 10 mins each, in DPBS-T, the membrane was incubated in a 1/500 dilution of HRP conjugated secondary antibody (goat anti-mouse IgG HRP, sc2031, 200µg/0.5 mL, Santa Cruz Biotechnology, Dallas, TX) in 10 mL of DPBS-T/2.5% BSA at room temperature with gentle shaking for 1 hr. After rinsing, the membrane was exposed to a chemiluminescent HRP substrate according to manufacturer's instructions and imaged with a Biorad ChemiDoc XRS+.

Results

Generation of Cx50 Mutants

A total of 10 different mutant Cx50 clones were generated to investigate the role of histidine residues located near the cytoplasmic mouth of the channel in conferring pH sensitivity to hemichannels. The choice of substitutions was partly guided by those used to demonstrate a role for H95 in pH-dependent gating of Cx43 gap junction channels (Ek et al, 1994). These included H95Q, H95Y, H95D, and H95K. In the Cx43 studies, the H95Q was interesting in that it created a nonfunctional channel that could be rescued by substituting a histidine into nearby positions. Given that Cx50 has two additional histidine residues near H95, namely H98 and H99, there was reason to believe that the Cx50 H95Q single mutation might remain functional. Likewise, substituting glutamine at other histidine positions in Cx50 should also produce functional channels due to remaining nearby histidines so the H98Q and H99Q mutants were generated to test this hypothesis.

The next goal was to isolate each individual histidine to test its specific role, and so double mutations were made to substitute two histidine residues in pairwise configurations,

leaving only one remaining histidine. Glutamine was used for these substitutions to be consistent with the single mutations above. In this way, if the site-directed mutagenesis did not work well with primers containing multiple nucleotide changes then the single mutant clones could be used as a starting point for additional rounds of single mutations. To test the roles of a specific individual histidine, the following mutants were constructed: H95Q-H98Q, H95Q-H99Q, and H98Q-H99Q, which left a single histidine in the triad.

Finally, to test whether or not pH-sensitivity was dependent on any histidine in the area, the triple mutant H95Q-H98Q-H99Q was made.

The forward and reverse primer sequences used to generate the above mutants are described in Table 3. These primers were determined using the Agilent QuikChange Primer Design tool (Agilent, Santa Clara, CA) and all resulted in amplification of the target DNA. The amplified plasmid DNA was Dpn digested to remove wildtype plasmid DNA and then used to transform XL10 Gold Ultracompetent E.Coli. An aliquot of the transformation reaction was plated on LB Agar-Amp plates and incubated at 37°C overnight resulting in a steak of growth with multiple individual colonies residing at the borders of the heavy growth region. Two colonies were isolated for each transformation reaction. Plasmid DNA was isolated from each colony for sequencing, with a subset of the clones shown in Figure 4.

Sequencing was performed by Integrated DNA Technologies (Coralville, IA) using a sequencing primer corresponding to the SP6 promoter region and an internal primer corresponding to a region in the cytoplasmic loop of Cx50. The use of the internal primer was needed to get complete sequence data to ensure no spurious mutations occurred. The nucleotide sequence data from each primer was overlapped and the full sequence was then translated using the ORFfinder tool (NCBI, national center for biotechnology information). Sequence

information verified successful substitutions in all mutants with the exception of H99Q. Of the twelve different mutants, H95Q, H95Y, H95K, H95D, H98Q, H98QH99Q2, H95QH98Q1, H95QH99Q1, H95QH99Q2, H95QH98QH99Q1, H95QH98QH99Q2 were verified via a Sp6 and a custom internal sequencing primer (internal sequencing primer was only used for the double and triple mutants to verify the Sp6 site following difficulties with sequencing). Portions of the translated sequence flanking the targeted region for the mutants are shown in Table 4.

Generation of Mutant cRNA

Plasmid from the verified mutants was isolated and linearized with EcoR1 prior to the cRNA synthesis reaction (Figure 5). I generated cRNA for each of the verified mutants using the Ambion mMessage mMachine Sp6 Kit (Ambion, Invitrogen, Carlsbad, CA), and used 1% agarose gel electrophoresis to confirm the presence and integrity of the RNA prior to injecting oocytes (Figure 6). Attempts were made to quantify the concentration of RNA with screentape machine and agarose gel such that the verified RNA injected into Xenopus oocytes was at a concentration to ensure that each oocyte received 5-10 ng of RNA, but the amount injected may have been less.

Functional Assays of Single Mutations

RNA generated for H95Q, H95Y, and wild-type Cx50 was injected into oocytes along with anti-Cx38 oligo RNA (5 ng) to suppress endogenous Cx38 expression. The H95D and H95K mutants remain to be tested. Injections were performed in calcium-free media, and oocytes were incubated at 17°C for 48 hours in supplemented ND96 to allow for expression of mutant proteins.

Oocytes expressing the desired protein were then voltage clamped using TEVC. The oocytes were perfused sequentially in solutions of high calcium (ND96) and low calcium (ND96

with no added divalent cations), and low calcium pH 6.0 (ND96 with no added divalent cations and pH 6.0). Channel activity was recorded from a holding potential of -20 mV and currents were elicited by imposing 3 sec voltage steps from -110 mV to +50 mV in 20 mV increments. Figure 7 shows the family of current traces elicited under these conditions for Cx50 WT, Cx50H95Q, Cx50H95Y, and Cx38 antisense-only injected oocytes. The currents recorded from Cx50 WT oocytes are typical of Cx50 hemichannels, whereby channels open at a holding potential of -20 mV when external divalent cations are removed but close at both depolarizing and hyperpolarizing voltage pulses. The currents recorded after perfusing with pH 6.0 media in absence of divalent cations are severely reduced, as is typical for Cx50 hemichannels (Beahm, 2002). The Cx50 WT currents serve as a positive control for my technique and the quality of cRNA. Oocytes injected only with Cx38 antisense oligonucleotide displayed no significant currents, indicating that the anti-Cx38 oligonucleotide is successfully inhibiting endogenous channels. Oocytes injected with cRNA coding for the single H95 substitutions, H95Q and H95Y, showed current patterns similar to that of wild-type, whereby the currents in low calcium could be blocked by reducing external pH to 6.0.

Whole-cell conductances were calculated from the current trace data and summarized in Figure 8. My Cx50WT displays typical behavior for Cx50, with minimal conductance at either high calcium or low calcium at pH 6.0, and high conductance at low calcium at pH 7.4. Interestingly, the single mutants H95Q and H95Y demonstrated a high mortality rate with significant nuclear migration as compared to the oligo and WT injected oocytes (also shown in Figure 8) and thus I was unable to obtain many replicates which led to large error bars. In some batches of oocytes, there were no surviving oocytes to record. This may be due to leakiness, an

incomplete block of hemichannel activity during incubation prior to recordings, or another property of the expressed protein.

Functional Assays of Double and Triple Substitutions

I then tested the individual role of each histidine with double substitution mutants and the effect of replacing all three histidines with a triple substitution mutant. cRNA was injected for these mutants along with anti-Cx38 oligo, and as above, injections were performed in calcium-free media, and oocytes were incubated at 17°C for 48 hours to allow for expression of mutant proteins. Although >10 oocytes were tested for each double and triple mutation, no significant hemichannel currents could be detected. A summary of conductance measurements across three different batches of oocytes are shown in Figure 9, which includes data from Figure 8 for comparison between WT and single mutants versus the double and triple mutants.

Detecting Plasma Membrane Cx50 by Western Blot

Following the lack of currents detected from oocytes injected with double and triple mutant cRNA, I quantified the level of expression by running a Western blot of biotinylated surface proteins from oocytes used to generate the data in Figure 9. This assay allowed us to determine the levels of channels specifically expressed in the plasma membrane, rather than those residing, and possibly trapped, in the ER or Golgi apparatus. This was accomplished by biotintylating surface proteins prior to homogenization. After biotintylation, whole oocytes were homogenized and solubilized and the biotintylated proteins were captured and purified using avidin beads. The purified biotintylated proteins were then separated by size on a denaturing SDS-PAGE gel and transferred to nitrocellulose to be probed with an anti-Cx50 antibody as part of a western blot technique. The results are shown in Figure 10. Only three bands were detected on the Western blot, and all at the expected size of 50 KDa. The left lanes show proteins isolated

from oocytes that were injected with Cx50 WT cRNA synthesized from two different WT clones. The MW standards (blue-stained proteins) were imaged separately from the same blot and overlaid on the figure. An approximately 50 KDa protein was detected in the Cx50 WT oocytes that generated visible hemichannel currents. Bands for two different double mutants, Cx50H95QH98Q and Cx50H98QH99Q, were not present, possibly due to poor expression or trafficking. However, the triple mutant, Cx50 H95QH98QH99Q, which showed little to no hemichannel conductance, did produce a 50KDa band. Hence, the absence of hemichannel current in the triple mutant could not be explained by the lack of plasma membrane resident protein. This protein may have not oligomerized correctly to form a hemichannel or did oligomerize but failed to form a functional hemichannel.

Discussion

Site-directed mutagenesis was used to successfully generate a set of Cx50 mutations aimed at determining the role of histidine residues in pH-dependent gating. These residues are located on the second transmembrane domain near the cytoplasmic mouth of the channel. Preliminary functional studies conducted in the Xenopus oocyte expression system suggest that the H95 conserved among all connexins may not be necessary for the pH dependence of these hemichannels. I found that substitution of H95 for either Y or Q did not result in a dramatic loss of pH sensitivity, although possible small shifts in pH sensitivity were not assayed. Hemichannel currents that can be elicited after removal of external divalent cations were severely reduced at an external pH of 6.0 as they are in wildtype Cx50. This implies that there is an alternative pH-gating mechanism in Cx50, as appears to be the situation for Cx46. This mechanism may involve either H98 and/or H99 acting as redundant receptor sites, or a hitherto unknown mechanism.

A topology map of Cx50 (Figure 2) shows the relative locations of the histidine residues near H95, and a helical wheel map of the second transmembrane alpha helix for Cx43, Cx46, and Cx50 reveals the importance of the positioning of the three histidine residues in Cx50 (Figure 3). When H95 in Cx43 was mutated to glutamine, a mutation of A94 to histidine rescued pH sensitivity, but the mutation of L93 to histidine did not (Ek et al, 1994). The helical wheel model shows that A94 is closer to H95, whereas L93 is located on the opposite side of the α-helix. Similarly, H95, H98 and H99 are situated on the same side of the helix in Cx50. If H98 and H99 can function similarly to the rescuing mutation in Ek et al, it would explain the retained pH sensitivity of my Cx50H95 mutants. Additionally, although not tested, H98 in Cx46 could serve a similar purpose, which would explain the failure of Trexler et al (1999) to attenuate pH sensitivity by the substitution of H95 with other residues. Further quantification of mutants and replication of these results should be undertaken to substantiate this hypothesis.

I investigated the specific role of the other histidine residues in Cx50's triad by generating double and triple mutants. However, hemichannel currents could not be detected in oocytes expressing these mutants, which may reflect either poor expression levels or trafficking issues or a structural change in the protein resulting from mutagenesis. This low expression level was also observed by Trexler et al, who noted that expression of Cx46 channels with H95 substitutions was substantially lower than that of WT. H95 may play an important structural role in the protein, which could explain the small currents and low expression levels for the double and triple mutants, as the channel may not be folded properly. Cx43 mutants that resulted in the absence of detectable channel currents were not studied at the protein expression level (Ek et al, 1994).

The absence of detectable channel currents could reflect an issue with the expression and trafficking of mutant proteins. I ran a Western blot of biotinylated surface proteins to determine if the double and triple mutants were unable to be translated and trafficked correctly, which would explain the lack of meaningful currents. No bands were detectable for the double mutants. This could reflect a number of possibilities, including poor cRNA quality, the inability to effectively translate the mutant cRNA, the inability to traffic the mutant protein to the plasma membrane, or extremely low expression levels due to insufficient cRNA levels. However, the triple mutant (H95Q+H98Q+H99Q) was easily detected, and in relatively higher amounts than wild-type Cx50. This may be an indication that the channel underwent structural changes due to the specific mutations, and as a result was either nonfunctional or has a greatly reduced conductance. A constriction of the central pore as a result of mutating more than one residue at the narrowest part of the channel could be an explanation for non-detectable to minimal currents. A Western blot of whole-cell homogenate should be run to determine if the double mutants are present within the oocyte but not being expressed on the surface. If bands are present for the mutants in whole-cell homogenate and not for biotinylated surface proteins, this would suggest a problem in trafficking rather than translation. And if bands are not detected, it could indicate a failure in the translation of the mutated cRNA.

Another area for future work is continued assessment of the H95Q and H95Y single mutants. As shown previously, expression of the H95Q and H95Y mutant proteins in oocytes produced pH-sensitive channels with current magnitudes comparable to WT, but also coinciding with high oocyte mortality. The high mortality is often associated with the expression of functional hemichannels that are not adequately maintained in a closed state. My early experiments did not include the use of $CoCl_2$ to help keep hemichannels closed. Although these

hemichannels closed upon reducing external pH to 6.0, behaving similarly to wildtype hemichannels, it remains possible that the H95 mutations altered the pH sensitivity to some extent. A proton dose-response curve should be constructed for these mutants to identify a possible shift in the pH sensitivity caused by the mutation.

The pH sensitivity of the single mutants suggests that H95 is not necessary for pH gating in Cx50. Mutants H95Q and H95Y displayed sensitivity to external pH 6.0 similar to that of wild-type. The hypothesis that the additional two histidines at positions H98 and H99 could serve as redundant sensors could not be adequately tested because the double mutants have not expressed well in oocytes. While the choice of glutamine as a substitution for histidine was partly based on prior published studies, it may have resulted in compromised channels that could not be properly translated and trafficked to the plasma membrane. Ongoing work includes testing other amino acid substitutions in the double mutants to hopefully generate functional hemichannels that can be used to assess the individual contributions of the different histidine residues.

The lens connexins, Cx46 and Cx50, apparently do not require the conserved H95 to remain very sensitive to pH and hence this specific residue does not serve as the sole "receptor" in the 'particle-and-receptor model' as laid out by Ek et al (1994). Furthermore, our lab has preliminary results demonstrating that truncation of the tail of Cx50 also does not drastically affect the pH sensitivity of Cx50 hemichannels (unpublished data). This is consistent with studies of Cx46 (Trexler et al, 1999). Hence it appears that pH sensitivity of the lens connexins results from an unidentified mechanism. This mechanism could still be based on the multiple histidine residues located at the cytoplasmic mouth of the channels. The physiological significance of pH sensitivity of lens gap junction channels and their component hemichannels

remains to be explored. This thesis is a first step to understand the mechanism of pH sensitivity and its structural determinants in hopes of manipulating channel behavior for future experiments.

Literature Cited

Bao, X., Altenberg, G. A., & Reuss, L. (2004). Mechanism of regulation of the gap junction protein connexin 43 by protein kinase C-mediated phosphorylation. *American Journal of Physiology - Cell Physiology*, *286*(3), 647-654.

Beahm, D. L., & Hall, J. E. (2002). Hemichannel and junctional properties of connexin 50. Biophysical Journal, 82(4), 2016-2031.

DeRosa, A. M., Mui, R., Srinivas, M., & White, T. W. (2006). Functional characterization of a naturally occurring Cx50 truncation. Investigative Ophthalmology & Visual Science, 47(10), 4474-4481

Duffy, H. S., Sorgen, P. L., Girvin, M. E., O'Donnell, P., Coombs, W., Taffet, S. M., Delmar, M., Spray, D. C. (2002). pH-dependent intramolecular binding and structure involving Cx43 cytoplasmic domains. Journal of Biological Chemistry, 277(39), 36706-36714.

Ebihara, L., & Steiner, E. (1993). Properties of a nonjunctional current expressed from a rat connexin46 cDNA in xenopus oocytes. The Journal of General Physiology, 102(1), 59-74.

Ek, J. F., Delmar, M., Perzova, R., & Taffet, S. M. (1994). Role of histidine 95 on pH gating of the cardiac gap junction protein Connexin43. Circulation Research, 74(6), 1058-1064

Ek-Vitorín, J. F., Calero, G., Morley, G. E., Coombs, W., Taffet, S. M., & Delmar, M. (1996). PH regulation of connexin43: Molecular analysis of the gating particle. Biophysical Journal, 71(3), 1273-1284.

Gao, J., Sun, X., Moore, L. C., White, T. W., Brink, P. R., & Mathias, R. T. (2011). Lens intracellular hydrostatic pressure is generated by the circulation of sodium and modulated by gap junction coupling. The Journal of General Physiology, 137(6), 507-520.

Gemel, J., Lin, X., Veenstra, R. D., & Beyer, E. C. (2006). N-terminal residues in Cx43 and Cx40 determine physiological properties of gap junction channels, but do not influence heteromeric assembly with each other or with Cx26. Journal of Cell Science, 119(Pt 11), 2258-2268.

Goldberg, G.S., Valiunas, V., Brink, P.R. (2004). Selective permeability of gap junction channels. Biochimica et Biophysica Acta (BBA) – Biomembranes, 1662(1-2), 96-101.

Gong, X., Li, E., Klier, G., Huang, Q., Wu, Y., Lei, H., Kumar, N.M, Horwitz, J., Gilula, N. B. (1997). Disruption of alpha3 connexin gene leads to proteolysis and cataractogenesis in mice. Cell, 91(6), 833.

Guan, B., Chen, X., & Zhang, H. (2013). Two-Electrode Voltage Clamp. Methods in Molecular Biology, 998, 79-89.

Harris, A.L., Locke, D. (2009). Connexins. A guide. New York, New York: Humana Press.

Hu, J., Fu, R., Nishimura, K., Zhang, L., Zhou, H., Busath, D. D., Vijayvergiya, V., Cross, T. A. (2006). Histidines, heart of the hydrogen ion channel from influenza a virus: Toward an understanding of conductance and proton selectivity. Proceedings of the National Academy of Sciences of the United States of America, 103(18), 6865-6870.

Kaptan, S., Assentoft, M., Schneider, H.P., Fenton, R., Deitmer, J., MacAulay, N., de Groot, B.L. (2015). H95 is a pH-dependent gate in Aquaporin 4. Structure 23, 2309-2318.

Kelly, J. J., Simek, J., & Laird, D. W. (2015). Mechanisms linking connexin mutations to human diseases. Cell and Tissue Research, 360(3), 701-721.

Li, J., Wang, Q., Fu, Q., Zhu, Y., Zhai, Y., Yu, Y., Zhang, K., Yao, K. (2013). A novel connexin 50 gene (gap junction protein, alpha 8) mutation associated with congenital nuclear and zonular pulverulent cataract. Molecular Vision, 19, 767-774.

Liu, J., Xu, J., Gu, S., Nicholson, B., Jiang, J. (2010). Aquaporin 0 enhances gap junction coupling via its cell adhesion function and interaction with connexin 50. Journal of Cell Science, 124(2), 198-2016.

Liu, S., Taffet, S., Stoner, L., Delmar, M., Vallano, M. L., & Jalife, J. (1993). A structural basis for the unequal sensitivity of the major cardiac and liver gap junctions to intracellular acidification: The carboxyl tail length. Biophysical Journal, 64(5), 1422-1433

Liu, Y., Qiao C., Wei, T., Zheng, F., Guo, S., Chen, Q., Yan, M., Zhou, X. (2015). Mutant connexin 50 (S276F) inhibits channel and hemichannel functions inducing cataract. Journal of Genetics, 94(2), 221-229.

Liska, F., Chylikova, B., Martinek, J., Kren, V. (2008). Microphthalmia and cataract in rats with a novel point mutation in connexin 50 - L7Q. Molecular Vision, 14, 823-828.

Mathias, R. T., Kistler, J., & Donaldson, P. (2007). The lens circulation. Journal of Membrane Biology, 216(1), 1-16.

Morley, G. E., Taffet, S. M., & Delmar, M. (1996). Intramolecular interactions mediate pH regulation of connexin43 channels. Biophysical Journal, 70(3), 1294-1302.

Németh-Cahalan, K. L., Kalman, K., & Hall, J. E. (2004). Molecular basis of pH and Ca2+ regulation of aquaporin water permeability. The Journal of General Physiology, 123(5), 573-580.

Paynter, J., Shang, L., Bollepalli, M., Baukrowitz, T., Tucker, S. (2010). Random mutagenesis screening indicates the absence of a separate H^+-sensor in the pH-sensitive Kir channels. Channels, 4(5), 390-397.

Peracchia, C. (2004). Chemical gating of gap junction channels; roles of calcium, pH and calmodulin. Biochimica et Biophysica Acta (BBA), 1662(1-2), 61-80.

Sáez, J. C., Retamal, M. A., Basilio, D., Bukauskas, F. F., & Bennett, M. V. L. (2005). Connexin-based gap junction hemichannels: Gating mechanisms. BBA - Biomembranes, 1711(2), 215-224

Sahu, G., & Bera, A. K. (2013). Contribution of intracellular calcium and pH in ischemic uncoupling of cardiac gap junction channels formed of connexins 43, 40, and 45: A critical function of C-terminal domain: E60506. PLoS One, 8(3)10.

Shahidullah, M., & Delamere, N. A. (2014). Connexins form functional hemichannels in porcine ciliary epithelium. Experimental Eye Research, 118, 20-29.

Srinivas, M., Kronengold, J., Bukauskas, F. F., Bargiello, T. A., & Verselis, V. K. (2005). Correlative studies of gating in Cx46 and Cx50 hemichannels and gap junction channels. Biophysical Journal, 88(3), 1725-1739.

Stergiopoulos, K., Alvarado, J. L., Mastroianni, M., Ek-Vitorin, J. F., Taffet, S. M., & Delmar, M. (1999). Hetero-domain interactions as a mechanism for the regulation of connexin channels. Circulation Research, 84(10), 1144-1155.

Tong, X., Aoyama, H., Tsukihara, T., Bai, D. (2014). Charge at the 46th residue of connexin 50 is crucial for the gap-junctional unitary conductance and transjunctional voltage-dependent gating. The Journal of Physiology, 592(23), 5187-5202.

Trexler, E., Bukauskas, F., Bennett, M., Bargiello, T., & Verselis, V. (1999). Rapid and direct effects of pH on connexins revealed by the connexin46 hemichannel preparation. Journal of General Physiology, 113(5), 721-742.

Wang, X., Xu, X., Ma, M., Zhou, W., Wang, Y., Yang, L. (2011). pH-dependent channel gating in connexin26 hemichannels involves conformational changes in N-terminus. Biochimica et Biophysica Acta, 1818, 1148-1157.

Wang, Z., & Schey, K. L. (2009). Phosphorylation and truncation sites of bovine lens connexin 46 and connexin 50. Experimental Eye Research, 89(6), 898-904. doi:10.1016/j.exer.2009.07.015

White, T. W., Goodenough, D. A., & Paul, D. L. (1998). Targeted ablation of Connexin50 in mice results in microphthalmia and zonular pulverulent cataracts. The Journal of Cell Biology, 143(3), 815-825

Xu, X., Berthoud, V. M., Beyer, E. C., & Ebihara, L. (2002). Functional role of the carboxyl terminal domain of human connexin 50 in gap junctional channels. Journal of Membrane Biology, 186(2), 101-112.

Ye, Z., Wyeth, M. S., Baltan-Tekkok, S., & Ransom, B. R. (2003). Functional hemichannels in astrocytes: A novel mechanism of glutamate release. Journal of Neuroscience, 23(9), 3588.

Zampighi, G. A., Loo, D. D., Kreman, M., Eskandari, S., & Wright, E. M. (1999). Functional and morphological correlates of connexin50 expressed in xenopus laevis oocytes. The Journal of General Physiology, 113(4), 507-524

Tables and Figures

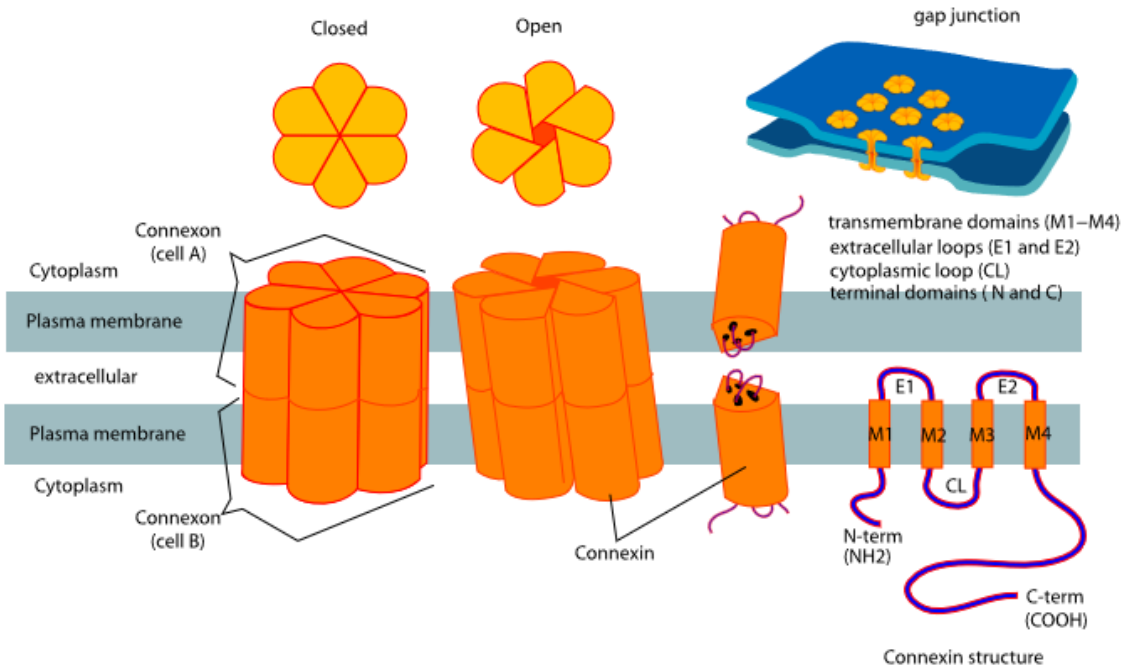

Figure 1: Gap Junction Structure and Connexin Membrane Topology

General structure of gap junction channels formed by the connexin transmembrane protein family. (Source: Wikimedia Commons)

Mouse Connexin (Mus Musculus)	Protein Sequence (Residues 90-105)
Cx50	LMYVG**H**AV**HH**VRMEEK
Cx46	LIYLG**H**VL**H**IVRMEEK
Cx45	MYLGYAI**H**KIAKMEHG
Cx43	LLYLA**H**VFYVMRKEEK
Cx40	LVYMG**H**AM**H**TVRMQEK
Cx37	LIYLG**H**VIYLSRREER
Cx32	LVAM**H**VA**H**QQ**H**IEKKM
Cx31	LVIL**H**VAYREERERKH

Table 1: Conserved Histidine Residues in Different Mouse Connexins

Partial amino acid sequence alignment in the region of H95 for different mouse connexins. Sequences taken from NCBI database.

Organism	Cx50 Protein Sequence (Residues 90-105)
Homo sapiens	LMYVG**H**AV**H**YVRMEEK
Macaca mulatta	LMYVG**H**AV**H**YVRMKEK
Canis lupus familiaris	LVYVG**H**AV**HH**VRMEEK
Mus musculus	LMYVG**H**AV**HH**VRMEEK
Rattus norvegicus	LMYVG**H**AV**HH**VRMEEK
Gallus gallus	LVYFG**H**AV**HH**VRMEEK
Danio rerio	LVYVG**H**AV**HH**VHMEEK
Xenopus tropicalis	LVYVG**H**AV**HH**VRMEEK

Table 2: Conserved Histidine Residues at Positions 95, 98, and 99 in Cx50 Orthologs

Partial amino acid sequence alignment in the region of H95 for Cx50 orthologs found in other species. Sequences taken from NCBI reference sequences for each species listed.

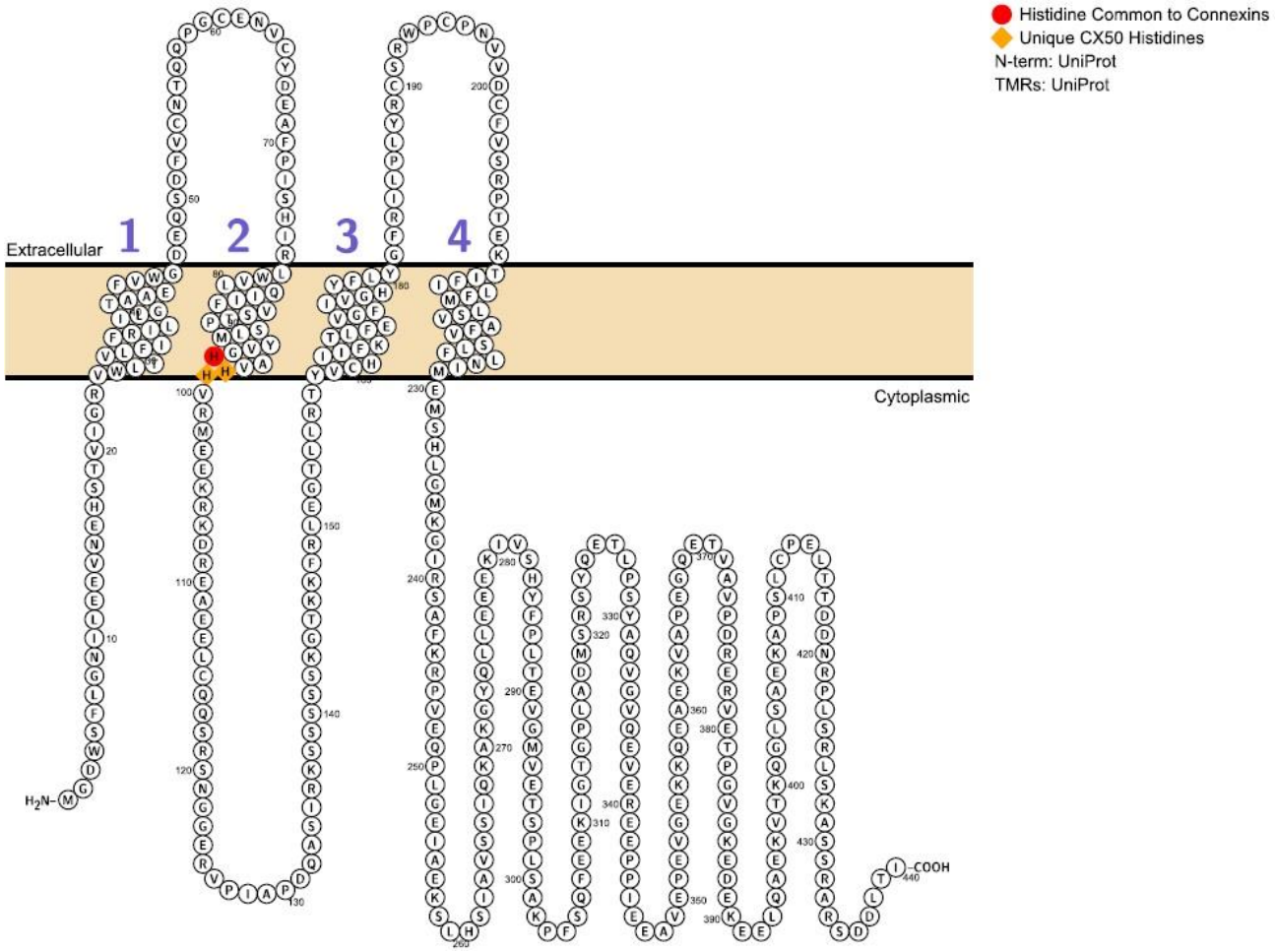

Figure 2: Primary Sequence and Membrane Topology of Mus musculus Cx50

Annotated model of *Mus musculus* Cx50 generated using Protter. Labeled histidine residues at the border of the second transmembrane domain and the first intracellular loop are sites of substitution by mutagenesis.

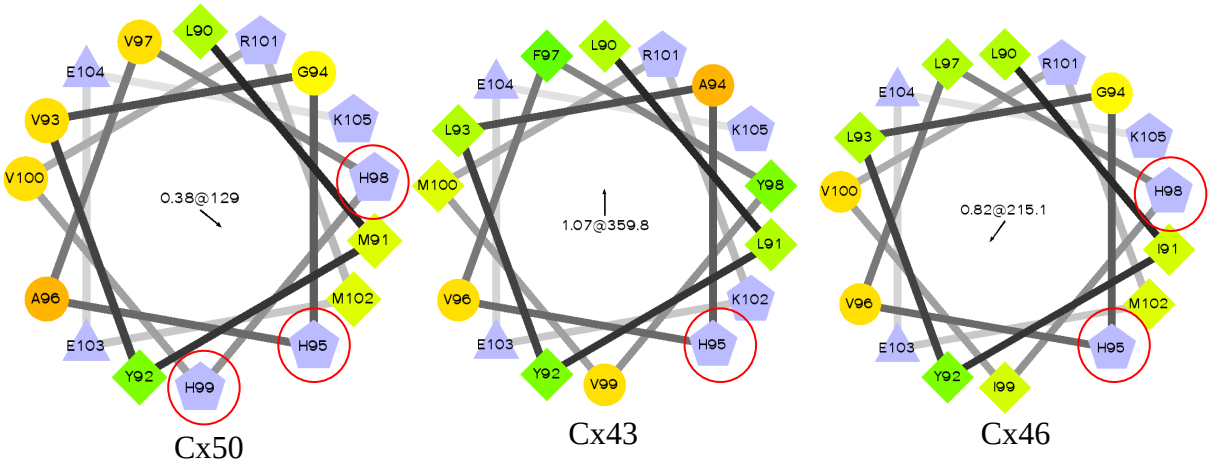

Figure 3: Comparison of Helical Wheel Models for Cx50, Cx43, Cx46

A helical wheel model of the second transmembrane domain of Cx50 is compared to that of Cx43 and Cx46. Histidine residues are circled in red for easy identification. The analysis reveals that the histidines H95, H98, and H99 in Cx50 are located on the same face of the helix. In Cx43, an H95Q substitution was nonfunctional but channel function and pH sensitivity was rescued by introducing a histidine at A94 which is shown to be on the same side of the helix as H95, but not rescued when the histidine was placed at L93 which exists on the opposite side. Cx46 is shown to indicate that there is a second histidine at position 98. Analysis done with Helical Wheel Projections, (http://rzlab.ucr.edu/scripts/wheel/wheel.cgi), Created by Don Armstrong and Raphael Zidovetzki. Version: Id: wheel.pl,v 1.4 2009-10-20 21:23:36 don Exp.

Mouse Cx50	nt: (5′)…ctgatgtacgtgggg**cac**gcggta**caccac**gttcgcatggaggagaag…(3′) AA: (90) L M Y V G **H** A V **H** **H** V R M E E K (105)	
Cx50 Mutant	Forward Primer (5’-3’)	Reverse Primer (5’-3’)
H95Q	atgtacgtgggg**cag**gcggtacaccac	gtggtgtaccgc**ctg**ccccacgtacat
H95Y	gatgtacgtgggg**tac**gcggtacaccacg	cgtggtgtaccgc**gta**ccccacgtacatc
H95D	atgtacgtgggg**gac**gcggtacaccac	gtggtgtaccgc**gtc**ccccacgtacat
H95K	ctgatgtacgtgggg**aag**gcggtacaccacgtt	aacgtggtgtaccgc**ctt**ccccacgtacatcag
H98Q	cgtggggcacgcggta**cag**cacgttcgc	gcgaacgtg**ctg**taccgcgtgccccacg
H99Q	cgtggggcacgcggtacac**cag**gttcgc	gcgaac**ctg**gtgtaccgcgtgccccacg
H95Q+H98Q	cgtgggg**cag**gcggta**cag**cacgttcgc	gcgaacgtg**ctg**taccgc**ctg**ccccacg
H95Q+H99Q	cgtgggg**cag**gcggtacac**cag**gttcgc	gcgaac**ctg**gtgtaccgc**ctg**ccccacg
H99Q+H98Q	cgtggggcacgcggta**cagcag**gttcgc	gcgaac**ctgctg**taccgcgtgccccacg
H98Q/H99Q/ H95Q	cgtgggg**cag**gcggta**cagcag**gttcgc	gcgaac**ctgctg**taccgc**ctg**ccccacg

Table 3: Custom Primer Design for Mutagenesis

Details of custom primer design. Partial Cx50 WT sequence, both Partial nucleotide (nt) and amino acid (AA) sequences obtained from NCBI Genbank database for Cx50 (mus *musculus*) are shown in the top row for reference. The amino acids of interest, H95, H98, and H99 and their corresponding codons are highlighted. Forward and reverse primers were designed using Agilent QuikChange Primer Design webpage to introduce nucleotide changes in codons of interest (highlighted) that would result in the amino acid substitutions listed under the “Cx50 Mutant” column.

Figure 3: Purified Mutant Plasmids for Sequencing.

Ethidium bromide stained plasmid DNA ran on 1% agarose gel at 100V for 20 minutes. Lanes from left to right: DNA ladder, H98Q1, H98Q2, H99Q1, H99Q2, H9598Q1, H9598Q2, H9599Q1, H9599Q2, H9899Q1, H9899Q2, H959899Q1, H959899Q2.

Cx50 Mutant	Cx50 Protein Sequence (Residues 90-105)
WT	LMYVG**H**AV**HH**VRMEEK
H95Q	LMYVG**Q**AV**HH**VRMEEK
H95Y	LMYVG**Y**AV**HH**VRMEEK
H98Q	LMYVG**H**AV**QH**VRMEEK
H98QH99Q	LMYVG**H**AV**QQ**VRMEEK
H95QH98Q	LMYVG**Q**AV**QH**VRMEEK
H95QH99Q	LMYVG**Q**AV**HQ**VRMEEK
H95Q H98Q H99Q	LMYVG**Q**AV**QQ**VRMEEK

Table 4: Sequencing Results for Different Cx50 Mutant Clones (AA sequence)

Translated mutant DNA sequence flanking the region of mutation in Cx50 WT and various mutant clones. DNA sequencing performed by Genscipt (Piscataway Township, NJ)..

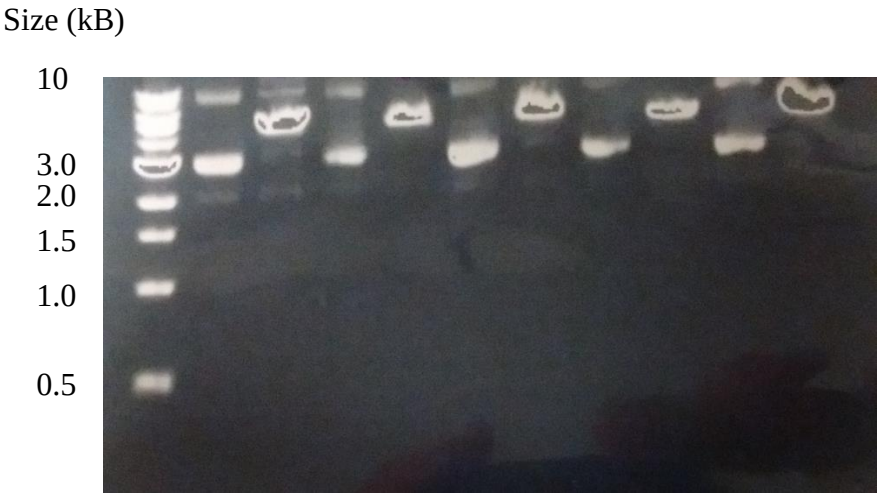

Figure 5: Linearization of Mutant Plasmids for cRNA Synthesis

EcoR1 Digest of Purified Plasmids Containing WT and Mutant Cx50. Lanes from left to right: Wildtype, digested wildtype, H98QH99Q, H98QH99Q digested, H95QH99Q, H95QH99Q digested, H95QH98Q, H95QH98Q digested, H95QH98QH99Q, H95QH98QH99Q digested.

A

B

Sample Table

Well	RINe	28S/18S (Area)	Conc. [ng/µl]	Sample Description
B1	9.4	1.8	527	2

C

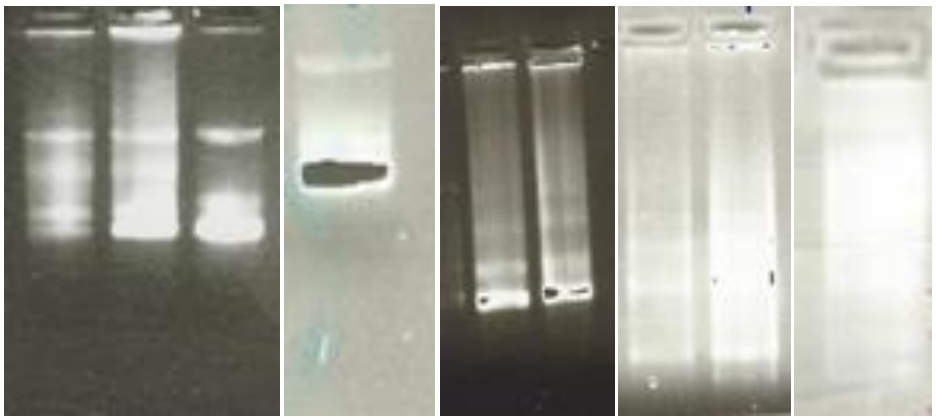

H95K H95D H95Q H95Y WT H9599Q H9598Q H959899Q H9899Q

Figure 6: Verification of RNA

Products of the cRNA synthesis reactions were ran on 1% agarose gel at 100V for 20 minutes to verify presence and integrity of synthesized cRNA. On some gels, estimates of cRNA concentrations, as shown in Panel A for Cx50 H95QH98Q (right lane) were based on a relative comparison to RNA markers (left lane). cRNA samples were sometimes ran on the Agilent Screentape machine, which produced concentration readouts as shown in Panel B for Cx50 H95QH98Q. Many times, cRNA was ran on agarose gels to simply verify presence and quality, as shown in Panel C for different Cx50 clones.

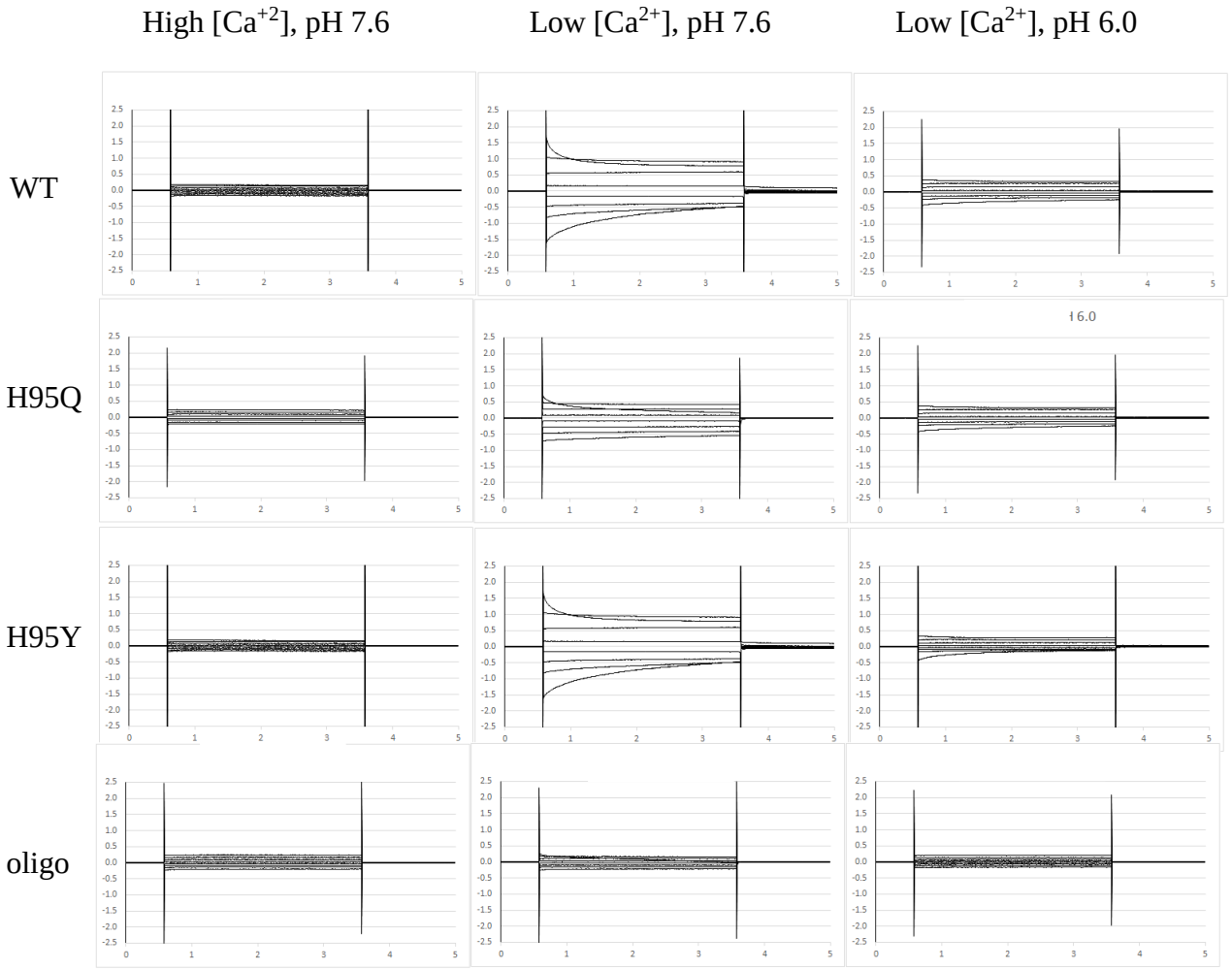

Figure 7: Representative Current Traces for Single Mutant Hemichannels

Representative current traces obtained from oocytes injected with cRNA of Cx50WT (top row), Cx50H95Q (second row), Cx50H95Y (third row) or anti-Cx38 oligonucleotide only (bottom row). Oocytes were held at a holding potential -20 mV and subjected to a series of 3 sec voltage steps from -110 mV to +50 mV in 20 mV increments. All current scales range from -2.5 to 2.5 uA for convenient comparison. Similar to Cx50 WT, both H95Q and H95Y exhibited open channels after removing divalent cations when the pH was 7.6 but showed dramatic decrease in hemichannel current when the pH was lowered to 6.0. Endogenous hemichannel currents were effectively eliminated by Cx38 antisense oligonucleotide.

A

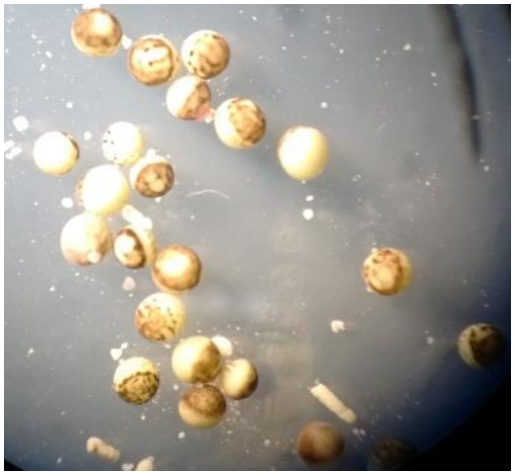

B

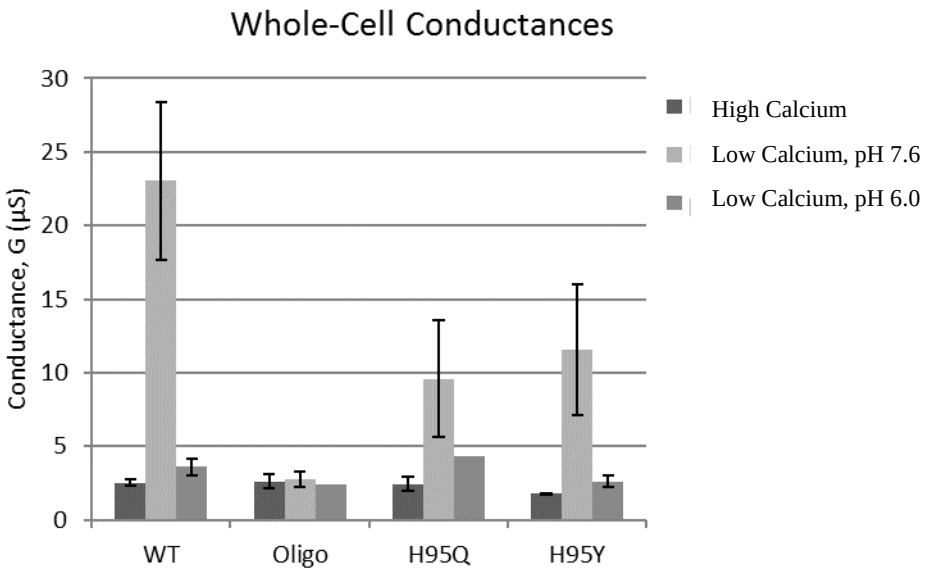

Figure 8: Expression of Functional Cx50 H95Q and H95Y Hemichannels

Top: Oocytes injected with ≥5 ng H95Q RNA, demonstrating blebbing and nuclear migration. Both H95Q and H95Y injected oocytes exhibited high mortality, which lead to the small number of replicates represented in the data. Bottom: Mean (+/- SE) of whole-cell conductance measured in High Calcium (> 2mM), Low Calcium, pH 7.6 (0 added divalent cations, pH 7.6), and Low Calcium, pH 6.0 (0 added divalent cations, pH 6.0) for oocytes expressing Cx50WT (n=5), Cx38 antisense Oligo only (n=2), Cx50H95Q (n=3), and Cx50H95Y (n=2).

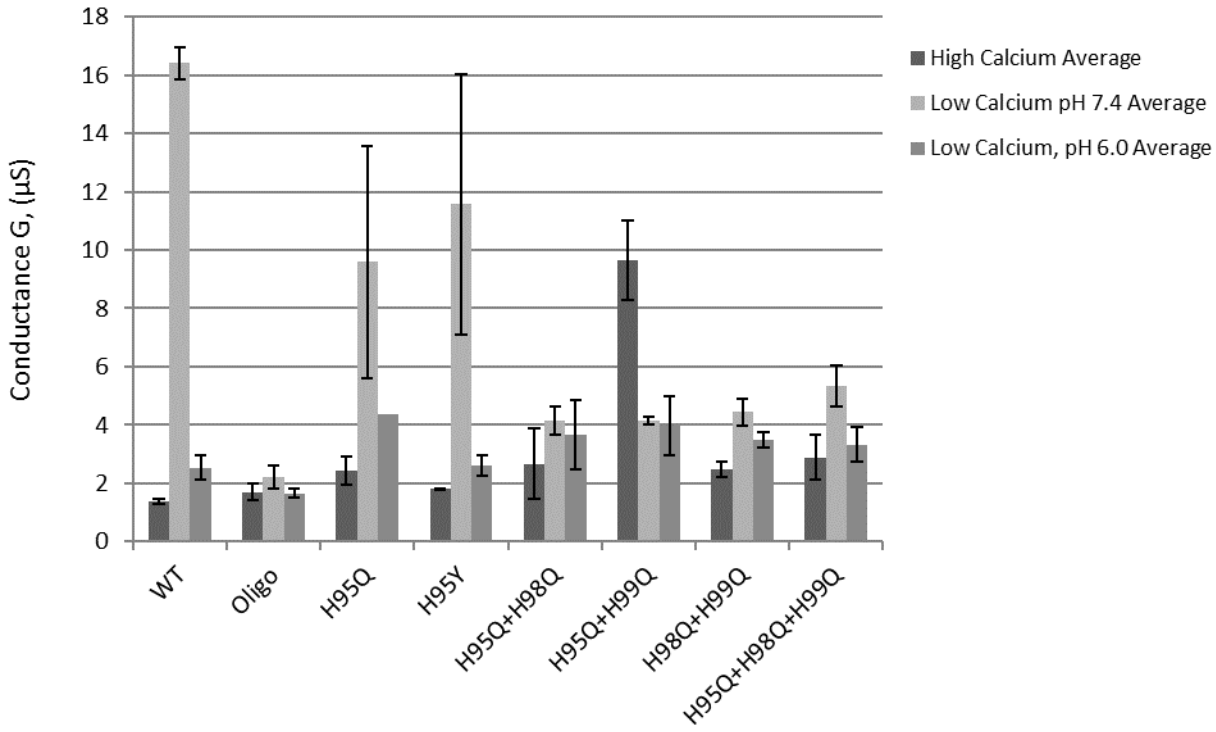

Figure 9: Summary of Whole Cell Conductance Measurements for Different Mutants

Whole-cell conductance of oocytes injected with ≥5 ng of each indicated RNA. N=3 for all mutants except for H95Y (N=2) and the low calcium pH 6 condition of H95Q (N=1). The double and triple mutants had low expression levels, and as such, there was no statistically significant difference between conductance measured at low and high calcium for these oocytes. The H95Q and H95Y mutants, however, demonstrated larger currents closer to wild-type magnitude. The H95Q+H99Q oocytes were generally leaky upon electrode impalement and membrane resistance increased over time during perfusions.

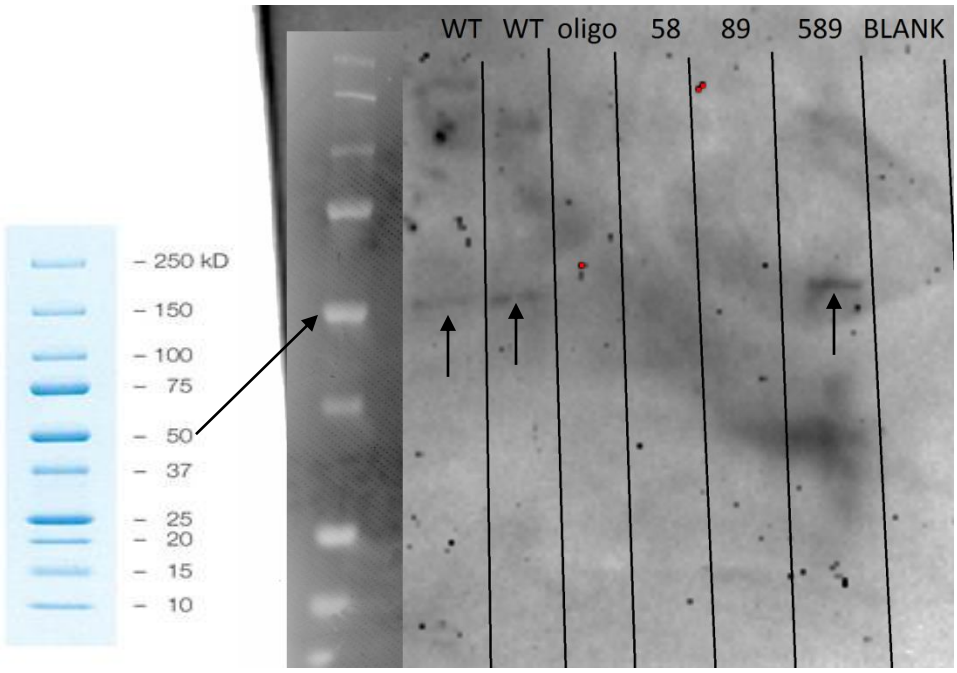

Figure 10: Western Blot of Surface-Labelled Proteins

Western Blot of surface labelled proteins probed with an HRP-conjugated anti-Cx50 monoclonal antibody and visualized with a luminol substrate. Each lane represents surface biotinylated protein collected from 6 oocytes 48 hours after injection with ≥5ng of indicated RNA. Abbreviated labels include WT = wildtype Cx50, oligo = Cx38 antisense only control, 58 = Cx50H95QH98Q, 89 = Cx50H98QH99Q, 589 = Cx50H95QH98QH99Q. Bands indicated by arrows are present at around the 50 KDa area for both the WT and triple mutant injected oocytes, but not for the double mutants or oligo controls. Left panel shows the MW profile of the pre-stained standard molecular weight markers used, which were imaged under different conditions on same blot and subsequently overlaid on the primary image.